

arXiv:astro-ph/0008209v3 1 Oct 2002

Acceleration by oblique shocks at supernova remnants and cosmic ray spectra around the knee region

K. Kobayakawa*

Fukui University of Technology, Gakuen 3-6-1, Fukui, Fukui, 910-8505, Japan

Y. S. Honda†

Department of Electrical and Information Engineering,

Kinki University Technical College, 2800,

Arima, Kumano, Mie, 519-4395, Japan

T. Samura

Department of Electrical and Computer Engineering,

Akashi National College of Technology,

679-3, Nishioka, Uozumi-cho, Akashi, 674-8501, Japan

(Dated: November 1, 2018)

Abstract

We examine the first order Fermi acceleration on the presumption that supernova remnant shocks cross ambient magnetic fields with various angles. These oblique shocks accelerate particles more efficiently than the parallel shocks and elevate the maximum energies achievable by the particles. The primary cosmic ray spectrum is strongly dependent upon these energies. We also consider the dependence of the injection efficiency and of spectral indices on obliquity. When indices and absolute fluxes at 10^{12} eV are given for six nuclear groups from balloon-borne data, each energy spectrum develops a smooth rigidity dependent knee structure. The resultant total spectrum also behaves similarly and fits well with ground-based experimental data up to several 10^{17} eV. It is shown as well that the chemical composition changes significantly from lighter to heavier nuclei as the energies of particles exceed the knee region. Other predicted curves are compared with the experimental data which they reproduce rather well.

PACS numbers: PACS 96. 40. De, 96. 50. Fm, 98. 70. Sa.

^{*}Electronic address: kobayakw@ccmails.fukui-ut.ac.jp

[†]Electronic address: yasuko@ktc.ac.jp

I. INTRODUCTION

In recent years, many measurements of the primary spectrum and chemical composition of cosmic rays have been carried out. Some of them are performed directly by balloon-borne experiments up to about 100 TeV. Others are by indirect ground-based experiments ranging from sub-TeV to some 100 EeV. These experiments have mainly been done to study the knee region. Recent reports indicate that the all-particle spectrum of cosmic rays does not present a sudden steepening, but rather a gradual bent near the energy at the knee, $E_{\text{knee}} = (2 - 5) \times 10^{15}$ eV, from $E^{-(2.6 \sim 2.8)}$ to $E^{-(3.0 \sim 3.2)}$ [1]. This value of E_{knee} is smaller than about a factor of 2 compared to those of earlier reports [2]. The chemical composition of cosmic rays below E_{knee} is directly measured and is almost constant in terms of the average logarithmic mass, $\langle \ln A \rangle$. However, the data of $\langle \ln A \rangle$ above E_{knee} fairly scatter, because they are obtained by indirect air shower observations. It is also noted that the value of $\langle \ln A \rangle$ varies depending on the hadronic interaction models assumed in simulations of extensive air showers [3].

On the other hand, it is generally believed that cosmic rays in the energy range up to E_{knee} are accelerated mostly by a supernova remnant (SNR) shock although there still exist some arguments that the origin of galactic cosmic rays (GCRs) is not yet settled [4]. When particles cross the shock front back and forth frequently, they obtain high energies proportional to the shock velocity, which is called the first order Fermi acceleration (for review, see [5]). This stochastic acceleration and deformation of source spectra due to energy-dependent diffusion from the galaxy can explain the power-law spectrum up to the knee. This scenario predicts that the maximum energy E_{max} , that particles can achieve by the shock acceleration mechanism, nearly equals E_{knee} .

Actually E_{max} is estimated to be $\sim 3Z \times 10^{13}$ eV [6] at most, where Z is the atomic number, which is nearly two orders lower than E_{knee} . However, this value is achieved by parallel shock acceleration where the normal of the shock front is parallel to the direction of the interstellar magnetic field. This is different from nonparallel shocks, where the angle α_1 between the shock normal and the field direction is not zero. These oblique shocks can accelerate particles much more efficiently [7, 8, 9]. For extremely oblique (quasiperpendicular) shocks, the values of E_{max} are increased by several orders of magnitude compared to those in parallel collisions. The details will be described in the next section.

In this paper we will explain the knee behavior of the energy spectrum with the acceleration mechanism as caused by oblique shocks. Our model is based on a simple idea as follows [10]. The ejected materials from a supernova explosion expand into the interstellar medium (ISM) driving a shock wave. While the expanding shell sweep up its own mass of the ISM, the shock acceleration may be active. The ejected mass ($\sim 10 M_{\odot}$) with large momentum moves out freely at constant velocity $10^8 - 10^9$ cm/s during the free expansion phase. The shape of the shock front is supposed to be almost spherically symmetric. The directions of the interstellar magnetic field lines will be, over a wide range, nearly random rather than well aligned. It is therefore assumed that the field lines meet the shock front at random angles α_1 , the cosines of which, η , are uniformly distributed. A more detailed discussion will be presented in section III. Since E_{\max} is strongly dependent upon η , E_{\max} values extend from $E_{\max}(\eta = 1) \equiv E_{\text{crit}}$ in parallel shocks to $E_{\max}(\eta = \eta_{\min}) \equiv E_{\text{cut}}$ in quasiperpendicular ones. The uniform distribution of η permits that particles with E , $E_{\text{crit}} < E < E_{\text{cut}}$, have less chances to reach high energies than those with $E \leq E_{\text{crit}}$.

There is an important question in acceleration at oblique shocks [11, 12, 13], however, namely that the rate of accelerated particles (injection efficiency) decreases drastically as the shock obliquity increases. On the other hand, the obliquity produces a harder energy spectrum [14, 15, 16, 17]. Since particles with $E < E_{\text{crit}}$ can be considered to be accelerated at shocks with the whole range of η , we do not apply modifications to the given spectra. For $E > E_{\text{crit}}$, both corrections of the injection efficiency and the change of the spectral index are taken into consideration, in addition to the chance probability of having η . Their fluxes decrease and cause a gradual change of spectral indices. In terms of rigidity, R_{crit} and R_{cut} , corresponding to E_{crit} and E_{cut} , are the same irrespective of Z . The flux of each elemental group starts to bend at different E_{crit} . Then the total flux shows a slow change around the knee.

We first choose the spectral indices and absolute fluxes for six nuclear groups at 1 TeV as an assumption so as to fit balloon-borne data. Next, based on our model, we calculate the energy spectrum up to 10^6 TeV for each group and obtain therefrom the total spectrum and energy dependence of the chemical composition directly. These results are compared with recent data of balloon and air shower experiments.

II. THE MAXIMUM ENERGY

In this section we estimate the maximum energy of particles accelerated by oblique shocks at supernova remnants. If magnetic field lines are not parallel to the shock normal, an electric field is induced in the rest frame of the shock. Particles drift along the shock front gaining energies due to this field. In order to describe the interactions of particles with shocks concisely, the de Hoffmann-Teller frame in which the electric field vanishes globally is widely used [18]. For oblique shocks, reflection at the shock front is more important than diffusion in the downstream region (Kirk & Heavens 1989 [19]), so that a more rapid acceleration can occur than for parallel shocks. The maximum energies of accelerated particles can be even a few orders of magnitude larger in the case of a quasiperpendicular shock compared to parallel ones.

Suppose a plane shock wave propagating at a non-relativistic speed U_1 with respect to the upstream medium. The shock normal intersects with the upstream magnetic field B_1 at an angle α_1 . A schematic view of the shock in the upstream rest frame is shown in Fig. 1. Parameters for the downstream region in its own rest frame, with magnetic field inclination β_2 and shock velocity U_2 , can be expressed in terms of the upstream ones [20]. We assume that the amplitude of the magnetic field perturbations is sufficiently small in the following calculation.

A. The dependence of E_{\max} on magnetic field inclination

There are some energy loss processes significant for the limitation of particle acceleration. For example, ionization, bremsstrahlung, and synchrotron radiation are conceivable. These processes for protons or other nuclei, however, are not so important within the energy range in which we are interested. The time scale of acceleration by oblique shocks at SNRs is regarded as sufficiently small compared to those of such loss processes.

Unless the energy losses of particles are significant, the finite lifetime of the supernova blast wave as a strong shock mainly limits the maximum energy per particle. Effective shock acceleration can occur until the swept up mass reaches the ejected mass $\sim 10 M_{\odot}$. The lifetime of the shock t_{sh} is estimated to be about thousand years for ejecta expanding at velocity $\sim 10^8$ cm/s into a medium of average density 1 proton/cm³. As long as the characteristic

length for diffusion is much less than the radius of the shock, the plane approximation is valid. Balancing the acceleration time scale with t_{sh} after Lagage & Cesarsky [21], we can write down the following expression for E_{max} ,

$$E_{\text{max}} = \frac{R_{\text{sh}}(r-1)}{rcx} U_1 e B_1 Z \left[\cos^2 \alpha_1 + \frac{\sin^2 \alpha_1}{x^2} + \frac{r(\cos^2 \alpha_1 + \frac{r^2}{x^2} \sin^2 \alpha_1)}{(\cos^2 \alpha_1 + r^2 \sin^2 \alpha_1)^{\frac{3}{2}}} \right]^{-1}, \quad (1)$$

where r is the compression ratio of the shock, i.e. $r = U_1/U_2$, and x is the square root of the ratio of κ_{\parallel} to κ_{\perp} : $x^2 = \kappa_{\parallel}/\kappa_{\perp}$, where the two κ 's are the parallel and normal components of the diffusion coefficient with respect to the magnetic field lines.

Substituting the various constants with plausible values, we obtain E_{max} as a function of $\eta (\equiv \cos \alpha_1)$ and x ,

$$E_{\text{max}} = 2.51 \times 10^{16} [\text{eV}] \left(\frac{B_1}{30 \mu\text{G}} \right) \left(\frac{R_{\text{sh}}}{3 \text{pc}} \right) \left(\frac{U_1}{10^7 \text{m/s}} \right) \frac{Z}{x} \frac{r-1}{r} \left\{ \eta^2 + \frac{1-\eta^2}{x^2} + \frac{r[\eta^2 + \frac{r^2}{x^2}(1-\eta^2)]}{[\eta^2 + r^2(1-\eta^2)]^{\frac{3}{2}}} \right\}^{-1}. \quad (2)$$

The maximum energy for parallel shocks ($\eta = 1$), E_{crit} can be estimated from Eq. (2) in the case of strong shocks ($r = 4$) with $x = 30$ and with typical values of B_1 , R_{sh} and U_1 ,

$$E_{\text{crit}} = 1.25 Z \times 10^{14} [\text{eV}]. \quad (3)$$

Here we evaluate the numerical value 2.51×10^{16} according to the recent papers. Namely, due to non-linear effects, the maximum energies are enhanced by the factor of $80/9$ compared to ordinary values [22]. We will comment on the rather large value of B_1 [23, 24] in the next subsection. It is noted that the value 1.25×10^{14} in Eq. (3) is larger than the usual ones $\sim 3 \times 10^{13}$.

It is also compared to Berezhko's values [22]. When an enhancement factor of $80/9$ is used, this value is larger by one order of magnitude, $\sim 1 \times 10^{15}$. Even if replacing the parameters of his Eq. (36), where the enhancement factor due to weak shock modification is $10/3$ by our typical values mentioned above and after the normalized value of the field 3 mG is corrected to 3 μG [25], we get $\sim 1.4 \times 10^{15}$. Thus in other words we may say that the value in Eq. (3) is only about ten times larger for field values used in a conventional derivation of E_{max} . Therefore numerical values in Eqs. (2) and (3) are not inadequate even if x has a strong effect.

In order to see how $E_{\max}(\eta)$ varies with different x values, $x = 10, 30, 100$ are tested since the value of x is considered to lie between 10 and 100. Other parameters are the same as the above ones. Figure 2 shows the η dependence of E_{\max} for $Z = 1$: proton. From Eq. (2), the value of E_{\max} is proportional to the particle charge Z . As shown in Fig. 2, the E_{\max} value is strongly dependent on the field inclination η . E_{\max} in quasiperpendicular shocks is larger than that in parallel shocks by two or three orders of magnitude for each value of x . In the case of $x = 30$, $E_{\text{cut}} = 1.84 \times 10^{17}$ eV is about 1470 times the value E_{crit} with $Z = 1$ in Eq. (3).

B. Magnetic field in the supernova remnants

As we have mentioned above, we take a B_1 -value somewhat larger than the average strength of the interstellar magnetic field of magnitude of microgauss. It is widely known that SNRs are usually accompanied with magnetic fields. The sufficiently strong field is possibly present in the accelerated region around SNR-shocks because of rapid expansion of ejecta into the interstellar medium. There is some possibility [26] that cosmic ray streams amplify non-linearly magnetic fields up to 1 mG. Recent measurement also suggest that some galactic SNRs possess intense magnetic fields of the order from milligauss to sub-milligauss in the downstream region [27, 28, 29, 30]. These observed values are suppressed by a factor of 5 or so in the upstream, and hence our choice $B_1 = 30 \mu\text{G}$ is quite relevant.

There are some investigations related to the magnetic field geometry in SNRs. In young remnants, the ambient field lines are stretched and amplified to be predominantly parallel to the shock normal on account of Rayleigh-Taylor instabilities [31]. On the other hand, for older SNRs perpendicular shocks likely originate from the compression of the ambient interstellar field. Observations of synchrotron radiation also support this morphology [32, 33]. The value of B_1 of our choice and isotropic distribution of η may be appropriate as far as we are concerned with the whole behavior of cosmic rays.

Here we also comment on another important parameter, x , which describes field fluctuation. In papers of Jokipii (1987) [7] and Ellison et al. (1995) [13], they use $\xi = \lambda/r_g$, which simply relates to x as $x^2 = \xi^2 + 1$ (In their original papers, they use the notation η instead of ξ but here we use ξ in order to distinguish it from our $\eta(\equiv \cos \alpha_1)$). $\xi \sim 1$ corresponds to the Bohm diffusion (strong scattering) limit and $\xi \rightarrow \infty$ when $\kappa_{\perp} \ll \kappa_{\parallel}$.

According to ref. [13], the x value is limited by $x \lesssim v/U_1$, where v is the particle velocity, and in quasi-perpendicular shocks $x \lesssim \tan \alpha_1$. Our choices $x = 30$ and $\eta_{\min} = 1/30$, which will be adopted later, however, do not satisfy the latter inequality. The fixed x value is also used for any η between η_{\min} and 1.

III. OUR MODEL

Based on the result that the angular dependence of the maximum energy is quite significant, we propose a simple model. The following three issues are examined: (1) the chance probability of η occurrence, (2) the dependence of the injection efficiency on η and (3) the η dependence of the spectral index.

A. Chance probability of η

The overall morphology of SNR-shocks is considered to be almost spherically symmetric even if the shape of each is somewhat distorted. The ambient disordered magnetic field lines over a wide range intersect the shock normal at various angles. Moreover, as we described in the section II. B, there exist SNRs with various ages whose magnetic fields cross the shock fronts with a wide variety of angles. Since both young and old SNRs are considered as sources of energetic cosmic rays, averaging over the various ages of SNRs and different shapes of their shock fronts, we assume a uniform distribution of η in our model.

The value of η is restricted within the range between η_{\min} and 1 to satisfy the condition that the shock front should not move at the light velocity or above in the H-T frame. The probability in the width $d\eta$ is then

$$f(\eta)d\eta = \frac{d\eta}{1 - \eta_{\min}} \quad (\eta_{\min} \leq \eta \leq 1), \quad (4)$$

where $\eta_{\min} = U_1/c \sim 1/30$ and $(1 - \eta_{\min})^{-1}$ is the normalization factor. The range where $0 \leq \eta < \eta_{\min}$ is neglected because it occupies only 1/30 of the whole η region. Let \mathcal{E} be the energy of a particle with $E_{\text{crit}} \leq \mathcal{E} \leq E_{\text{cut}}$. E_{crit} and E_{cut} are the maximum energies in parallel ($\eta = 1$) and extremely oblique (quasiperpendicular: $\eta = \eta_{\min}$) shocks, respectively. A particular value of η corresponds to an unique \mathcal{E} since $E_{\max}(\eta)$ is a monotonic decreasing function of η as shown in Fig. 2. Only oblique shocks in the range from the η to η_{\min} can then serve to give \mathcal{E} . The fluxes at \mathcal{E} should therefore be reduced by the factor $(\eta - \eta_{\min})/(1 - \eta_{\min})$.

B. Injection efficiency

Baring, Ellison and Jones [11, 34] developed test particle Monte-Carlo simulations with large angle scattering processes (abbreviated as LA). They showed that the efficiency for injecting thermal particles into an acceleration mechanism strongly depends on obliquity and varies inversely with α_1 (Θ_{Bn1} in their notation), in the case of high Mach numbers. They also checked the ξ (\approx our x) dependence of the injection efficiency, $\epsilon(\eta)$. When their results are applied to the present case $x \approx 30$, the injection efficiency relative to $\eta = 1$ is nearly equal to or less than 0.01 at $\eta = 0.6$. Namely oblique shocks with η from η_{\min} to 0.6 contribute very little to the acceleration of particles.

Naito and Takahara [16, 17] also attempted test particle simulations in oblique shocks. Instead of directly presenting $\epsilon(\eta)$, they showed the pitch angle (μ) distribution in both cases of LA and pitch-angle scattering (abbreviated as PA) in their figures 3 and 4 [17], respectively, for $\eta = 1.0, 0.75, 0.5, 0.25$. Using the number of injected particles for these η values, we can estimate $\epsilon(\eta)$ by integrating with respect to μ from -1 to 1 in the downstream, where the μ distribution of their simulation agrees well with the expected one [16]. The relative injection efficiency $\epsilon(\eta)$ changes little even if the number of accelerated particles in the upstream are added, because the numbers are less than those in the downstream and also the ratios to $\eta = 1.0$ are similar to those in the upstream.

For LA, $\epsilon(\eta) = 1, 0.73, 0.49, 0.26$, whereas for PA $\epsilon(\eta) = 1, 0.81, 0.59, 0.31$ are evaluated corresponding to $\eta = 1, 0.75, 0.5, 0.25$, respectively. It is argued [35] that LA is adequate for $\frac{\delta B}{B} \sim 1$, while PA is acceptable for $\frac{\delta B}{B} < 0.1$. In our case, $(\frac{\delta B}{B})^2 \sim \frac{1}{x} = \frac{1}{30}$ is somehow between LA and PA, and $\epsilon(\eta)$ is similar in both cases. Therefore, we may simply take,

$$\epsilon(\eta) = \eta \tag{5}$$

The detailed reason why the above two works present very different results on $\epsilon(\eta)$, is not clear. The input for simulations, however, differs for the two approaches. In Ellison et al. [13, 36], injected particles are thermal, the energies of accelerated particles are up to about 10 MeV, and U_1 is slow, say 5×10^5 m/s. Ellison has also presented the application to the real SNR [37]. He considered somewhat older objects which are in Sedov phase. On the other hand, in Naito and Takahara [17], the Lorentz factors of injected particles are fixed at 2, the factors of accelerated particles are followed up to 10^5 , and the shock is relativistic:

$U_1 \sim 0.1c$. In the light of the present treatments or parameters, such as $U_1 = 10^7$ m/s and considering that the energies concerned are higher than 1 TeV, we assume Eq. (5) here.

C. Change of spectral indices

In this subsection, we consider the dependence of the spectral index on obliquity. It has been frequently pointed out that one of the advantages of the first order Fermi acceleration mechanism is that it gives a power-law energy spectrum. Namely one gets for the differential spectrum dJ/dE , if we take terms of fluid velocities up to first order into account,

$$\frac{dJ}{dE} \propto E^{-q} \quad \left(\text{with} \quad q = \frac{r+2}{r-1} \right). \quad (6)$$

For a strong shock ($r = 4$), the differential spectral index is $q = 2$. This index is expected to be modified into the final index γ which is observed. γ is somewhat steeper than q by considering the energy-dependent leakage from the galaxy [38]. We do not go into detailed discussions of this change in this paper, even though different modifications are used for different nuclear groups in the next subsection.

This dependence of q values on η is examined. This dependence is assumed to apply to γ in the same form. Although nonlinear back reaction effects of accelerated particles reduce q values by about 0.5 at higher energies even in parallel shocks [39], only the index dependence on η is considered here. The dependence has been studied in earlier works [14, 15]. Here, we again refer to Naito and Takahara [16, 17]. In ref. [16] they showed that q is practically 2 at $\eta = 1$, and diminishes as η decreases except for $\eta \approx \eta_{\min}$ being rather independent for the three cases $\frac{U_1}{c} = 0.01, 0.03, 0.1$. It is also shown [17], for $\frac{U_1}{c} = 0.1$ in the case of LA, q is 2.08, slightly larger than 2, at $\eta = 1$, and almost linearly decreases as η decreases. Then q reaches a minimum of 1.5 at $\eta \approx 0.15$. For $\eta_{\min} < \eta < 0.15$, q starts to increase rapidly. While for the PA case, q is nearly equal to 2.1 at $\eta = 1$. As η decreases, q decreases monotonically and reaches 1.0 as η approaches η_{\min} . In both cases the energy spectra become harder as shocks are more oblique.

We choose the LA model except for $\eta \approx \eta_{\min}$ and assume simply that q is proportional to η such as,

$$q(\eta) = a\eta + b \quad (1 < \eta < \eta_{\min}), \quad (7)$$

where $a = 0.68$, $b = 1.41$ and $\eta_{\min} = \frac{1}{30}$. This dependence of power indices on obliquity

enhances intensities of accelerated particles by oblique shocks. The present choice leads to an underestimate of this enhancement. For the energies of particles \mathcal{E} less than E_{crit} , the enhancement factor should be unity, because of q levelling off by summing up over the whole region of η , i.e. from 1 to η_{min} .

For $E_{\text{crit}} < \mathcal{E} < E_{\text{cut}}$, there is a one-to-one correspondence of η to \mathcal{E} as mentioned above. Taking into account the injection efficiency given by Eq. (5), we introduce a correction factor

$$\zeta(\eta) = \frac{2}{1 - \eta_{\text{min}}^2} \int_{\eta_{\text{min}}}^{\eta} \eta' \left(\frac{\mathcal{E}}{E_{\text{crit}}} \right)^{-q(\eta') + q(\eta_a)} d\eta', \quad (8)$$

where $\eta_a = (1 + \eta_{\text{min}})/2$ is the average value of η . The factor $-q(\eta') + q(\eta_a)$ leads to a deviation of indices between $1 \sim \eta_{\text{min}}$ and $\eta \sim \eta_{\text{min}}$ and hence, b in Eq. (7) is cancelled. When $\mathcal{E} = E_{\text{crit}}$, that is to say $\eta = 1$, $\zeta(\eta = 1) = 1$ due to the normalization factor $\frac{2}{1 - \eta_{\text{min}}^2}$. The η dependence of indices compensates partially the injection efficiency but not completely. So $\zeta(\eta)$ is less than unity such as for $\eta_{\text{min}} < \eta < 0.8$, $0.7 < \zeta(\eta) < 0.8$.

In addition to $\zeta(\eta)$, the chance probability of η given by Eq. (4) should be combined. Since the probability is independent of $\zeta(\eta)$, after integrating Eq. (4) we obtain a final correction factor:

$$g(\eta) = \frac{\eta - \eta_{\text{min}}}{1 - \eta_{\text{min}}} \zeta(\eta) \quad (9)$$

In Fig. 3, $\zeta(\eta)$, $\frac{\eta - \eta_{\text{min}}}{1 - \eta_{\text{min}}}$ and $g(\eta)$ are sketched as dashed, dotted and solid curves, respectively.

In summary, the differential energy spectra can be expressed as:

$$\begin{aligned} \frac{dJ}{dE} &= CE^{-\gamma} & (E < E_{\text{crit}}) \\ &= CE^{-\gamma} g(\eta) & (E_{\text{crit}} \leq E \leq E_{\text{cut}}) \\ &= 0 & (E_{\text{cut}} < E), \end{aligned} \quad (10)$$

where C and γ are fixed according to six nuclear groups in the next section. E_{crit} is given by Eq. (3) and $E_{\text{cut}} = 1.84Z \times 10^{17}$ eV. From Eq. (10), one can see that the curve of the flux is differentiable changing from linear to a smooth bent above E_{crit} in a log-log diagram.

The velocity of the shock front becomes superluminal in the H-T frame in the region $0 \leq \eta < \eta_{\text{min}}$, which we have neglected. If particles are accelerated effectively by some other special mechanism, however, we should take this range into consideration.

IV. RESULTS

We calculate differential fluxes of various mass groups. The obtained fluxes are multiplied by $E^{2.5}$ in order to clarify the change of the spectral indices. The multiplied flux for each chemical component is normalized to the experimental data at $E = 1$ TeV, where E is the total (mass plus kinetic) energy per particle, to give

$$\Psi = \left[E^{2.5} \frac{dJ}{dE} \right]_{E=1\text{TeV}} = \phi E^{-\beta}, \quad (11)$$

where $\beta = \gamma - 2.5$. Here we take as an assumption two different types of values of Ψ and β as shown in Table I. Parameters with subscript “HEGRA” have been taken from the analysis of the HEGRA air shower experiment [40] and slightly modified such that the heavy and very heavy nuclei (HVH) parts are separated into Ψ of sub-Fe and Fe with the ratio 0.125 to 1.0 and with the same β . The values with suffix “Ours” have been determined so as to fit well various experimental data around $E = 1$ TeV.

We do not discuss in detail why some different values of Ψ and β are taken for groups of elements as in Table I. The most notable difference of these two models is the exponent β of the Fe spectrum. The resultant all-particle spectrum with “HEGRA” parameters shows a more rapid decrease for high energies. Since $x \sim (B/\delta B)^2$ which is estimated to be between 10 and 100, for simplicity, we fix hereafter the value of x at about its geometrical mean of $x = 30$ in the calculation of Eq. (1).

A. The energy spectra of primary cosmic ray components

In Fig. 4 we plot the calculated spectra of p and He against the kinetic energy E_k per nucleon. The theoretical spectra with “Ours” parameters are expressed by solid curves and those with “HEGRA” parameters by dashed ones. The energy spectrum of p starts to bend due to the g factor in Eq. (10) at the energy: $E_{k,\text{crit}}(\text{p}) \simeq 1.25 \times 10^5$ GeV/n. This steepening of the spectral index is visible in the recent data of the Tibet air shower experiment [42, 43, 44]. Here we cite the data of Tibet (2001) labelled proton dominant (PD) model in their paper. But their results from heavy dominant model are almost the same with those from PD. For He, $E_{k,\text{crit}}(\text{He}) = Z(\text{He})/A(\text{He}) \times E_{\text{crit}}(\text{p}) - m_{\text{p}} \simeq 6.3 \times 10^4$ GeV/n. JACEE data [46] seem to be consistent with this $E_{k,\text{crit}}(\text{He})$, while RUNJOB’s fluxes [41] are somewhat lower but their highest E_k does not reach $E_{k,\text{crit}}(\text{He})$.

We also present spectra of the CNO, middle, and Fe-group in Fig. 5. “middle” corresponds to the NeMgSi-group and the Fe-group to our “sub-Fe” plus “Fe” in Table I. The two types of curves are defined by the same notation as in Fig. 4. The fluxes of middle and those of Fe-group have been downscaled by factors of 10 and 100 with respect to the original values, respectively. The slow changes of spectral indices of these groups above $E_{k,\text{crit}} \simeq 6.3 \times 10^4$ GeV/n for CNO and 6.2×10^4 GeV/n for middle are not clearly seen from the data, because it is difficult to obtain such data by direct observations.

For Fe, $E_{k,\text{crit}} \simeq 5.8 \times 10^4$ GeV/n, the JACEE point with the highest energy ($\simeq 10^5$ GeV/n) shows a large value but with a large error. On the other hand, the recent Tibet data around $E_k \simeq 10^6$ GeV/n [47] show that the spectrum is constant or has only a small bent in the diagram of Fig. 5. This favors Ours choice over HEGRA’s.

We plot the theoretical curves of spectra for various nuclear groups with Ours choice of parameters versus the total energy per particle in Fig. 6. One can see that the spectra of lighter nuclei start to bend at lower energies. This is just due to Eqs. (2) and (10). Namely, the changes occur at a fixed rigidity of 1.25×10^5 GV as shown in Eq. (3). Summing the fluxes of all these groups, we obtain the flux of all particles which is plotted as “total” in this figure. Since the spectra of each group are smooth (differentiable) as mentioned above, the total spectrum should also be smooth. The knee behavior in our model comes from the η -dependence of E_{max} due to the oblique shock acceleration expressed in the second line of Eq. (10). This is different from the HEGRA analysis [49], Biermann [50], Stanev et al. [51] and Erlykin and Wolfendale [52]. In the first paper, the knee is explained by introducing an artificial break of slope at a fixed rigidity. The authors of the next two papers, interpret the knee as the superposition of sources from different phases of SNRs. In the last reference, the authors argue that a sudden steepening at the knee and the explosion of a single, recent, nearby supernova is most likely to explain cosmic rays around the knee.

In Fig. 7 the two curves of the total flux, i. e. with Ours (the same as in Fig. 6) and HEGRA choices of parameters, are compared with experimental data. As seen in this figure, Ours curve fits well Tibet [47] and Akeno data [53] up to several times 10^8 GeV, while the curve with HEGRA parameters is in good agreement with DICE [54, 55] and CASA-MIA [56], in which both E and Ψ are about 30% lower than the Akeno data. The KASCADE experiment presented a preliminary result with a four component assumption (H, He, C, and Fe) [57]. It is shown that the position of the knee depends on rigidity. That is also

one of our conclusions. Anyway, the total flux can be explained at least up to 10^8 GeV by the present model. Above that energy, the solid curve falls below the AKENO data. Other sources than SNRs in Galaxy may be needed.

We express the two curves in Fig. 7 in single power laws below and above E_{knee} by using the least square method. For HEGRA and Ours choices $\gamma = 2.713 \pm 0.006$ and 2.664 ± 0.002 , respectively, between 1.5×10^5 GeV and 1.5×10^6 GeV; and $\gamma = 3.248 \pm 0.012$ and 3.092 ± 0.008 , respectively, between 6×10^6 and 6×10^8 GeV are obtained. These values depend on the adopted energy range; but they can be compared with experimental data. For example, Tibet γ [1] gives 2.60 ± 0.04 below and 3.00 ± 0.05 above E_{knee} and CASA-BLANCA [3] 2.72 ± 0.02 and 2.95 ± 0.02 .

B. The energy dependence of chemical composition

Using the results of energy fluxes, we examine how the chemical composition of cosmic ray particles changes with energy. In Fig. 8 the flux ratio of p plus He to all particles is plotted against the energy per particle. Theoretical curves suggest a change with increasing energies from mixed composition to heavy particle dominance. The curve with HEGRA parameters lies almost within the uncertainties of experiments quoted here. The relative abundance of light elements, however, tends to increase again beyond the energy of several times 10^6 GeV from experiments of DICE and HEGRA.

As a commonly used indicator of the composition, we take the average value of the logarithm of the mass number A , as

$$\langle \ln A \rangle \equiv \frac{\sum_i f_i (\ln A_i)}{\sum_i f_i}, \quad (12)$$

where f_i is the flux of species i which denotes each elemental group as shown in Table I. Our two curves of $\langle \ln A \rangle$ versus energy E are shown and compared with various data in Fig. 9. Both curves monotonically increase with energy, which is naturally confirmed by the present model. The HEGRA parametrization gives lower values than Ours in the whole energy range.

In Fig. 8 experimental data scatter and have large uncertainties especially near and above the knee. A similar trend is seen in Fig. 9. This is due to the fact that ground-

based measurements can study the composition only indirectly. The values of $\langle \ln A \rangle$ significantly depends on the experimental observables to be treated and on the hadronic interaction models to be used in simulation processes. Fairly different $\langle \ln A \rangle$ values are reported by various groups. Some authors [54] say that $\langle \ln A \rangle$ decreases in energy regions higher than the knee. Other authors [3] show that $\langle \ln A \rangle$ has even a dip near E_{knee} . Most of the other data indicate that $\langle \ln A \rangle$ increases with E . Preliminary results of the KASCADE experiment [57] show a sharp increase in logarithmic mass above several times of 10^6 GeV. On the other hand, the data extracted from equi-intensity curves depicted by Chacaltaya II [65] are somewhat closer to Ours. In the present stage we cannot reach a definite conclusion about whether our curves are in good agreement with data or not.

V. CONCLUDING REMARKS

We consider the acceleration caused by oblique shocks in which outer magnetic field lines cross the shock normal at any angle α_1 . We calculate E_{max} as a function of $\eta = \cos \alpha_1$, where E_{max} is the maximum energy that particles can achieve (see Eq. (2)). It is shown that E_{max} with extreme obliquity is more than 1400 times compared to that with parallel shocks ($\eta = 1$). In the present model, η is distributed uniformly and the η dependence of the injection efficiency and the change of spectral indices are taken in to account. We choose the two parameter sets of power indices and absolute fluxes at 10^{12} eV for various elemental groups shown in Table I. Then the spectra and compositions of cosmic rays are calculated up to much higher energies, say $\sim 10^{17}$ eV. It is shown that $E_{\text{crit}} = 1.25Z \times 10^{14}$ eV, where spectral curves start to bend over and continue up to $E_{\text{cut}} \simeq 1470 \times E_{\text{crit}}$. These results fit the proton spectrum well and explain a smooth knee behavior around 3×10^{14} eV (see Fig. 4).

As to the total flux, both curves in Fig. 7 exhibit a smooth knee behavior. The “HEGRA” choice fits well DICE and CASA-MIA data, while “Ours” choice reproduces well Tibet and Akeno data up to several times 10^{17} eV. However, since our model is limited by E_{max} , for energies higher than $\sim 10^{17}$ eV, more energetic sources of cosmic rays should be necessary. Favorite candidates for the sources of cosmic rays far above the knee may be microquasars, pulsars, active galactic nuclei [66], gamma-ray bursts (GRBs) [67] or other hitherto unknown sources.

As for the composition, our value of $\langle \ln A \rangle$ increases with the energy per particle as shown in Fig. 9. Data from various experiments scatter and have large uncertainties, particularly above E_{knee} . Thus the situation remains uncertain. Recent results by Fly's Eye, Haverah Park, and HiRes groups provide some interesting data of composition in the high energy region above 10^8 GeV as summarized in ref. [61]. Data of Haverah Park and HiRes show that light components are abundant towards 10^9 GeV, while a relatively heavy composition is suggested by Fly's Eye. These may also suggest some other origins apart from SNRs.

In the present paper, we fixed x , B_1 , R_{sh} , r and U_1 (i. e. η_{\min}) in Eq. (2) to evaluate the dependence of E_{\max} on η quantitatively and to obtain numerical values which could be directly compared with data. Generally, there are various shocks at SNRs where these quantities differ considerably depending on their ages, sizes and so on. However, as far as we are concerned with the whole or averaged behavior of cosmic rays which are observed, our choices and fixing of these quantities seem to be appropriate. We neglect the extremely quasi-perpendicular case in which the de-Hoffmann-Teller frame cannot be used. These are problems remaining to be solved.

Acknowledgments

We are indebted to T. Shibata at Aoyama Gakuin University for informing us of RUN-JOB's data. We thank S. Ogio at Tokyo Institute of Technology for presenting the new Chacaltaya data. We are also grateful to T. Naito at Yamanashi Gakuin University for his many useful comments. We would like to thank C. Grupen at Siegen University for carefully reading the manuscript and correcting many mistakes.

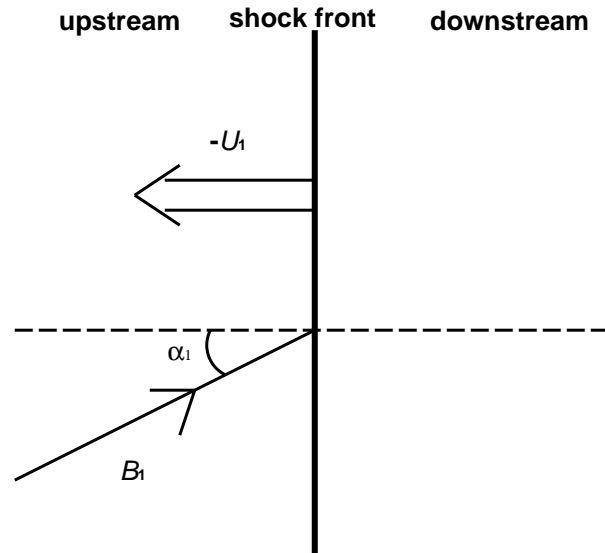


FIG. 1: A schematic diagram of an oblique shock in the upstream rest frame where the magnetic field B_1 intersects the shock normal at a nonzero angle α_1 .

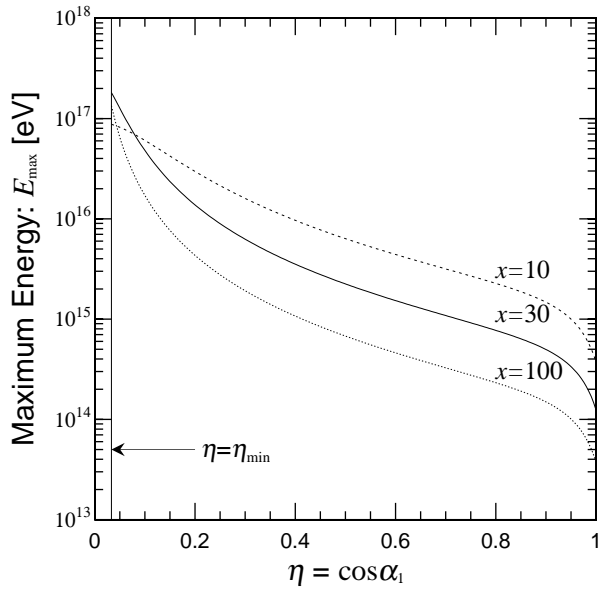


FIG. 2: The maximum energy E_{\max} for a proton with three values of x versus magnetic field inclination η . α_1 is an angle between the magnetic field and the normal of the shock front. The E_{\max} at $\eta = 1$ and $\eta = \eta_{\min}$, are the energies obtained by parallel shock and quasiperpendicular shock acceleration, respectively. For the nucleus with the atomic number Z , E_{\max} should be multiplied by Z .

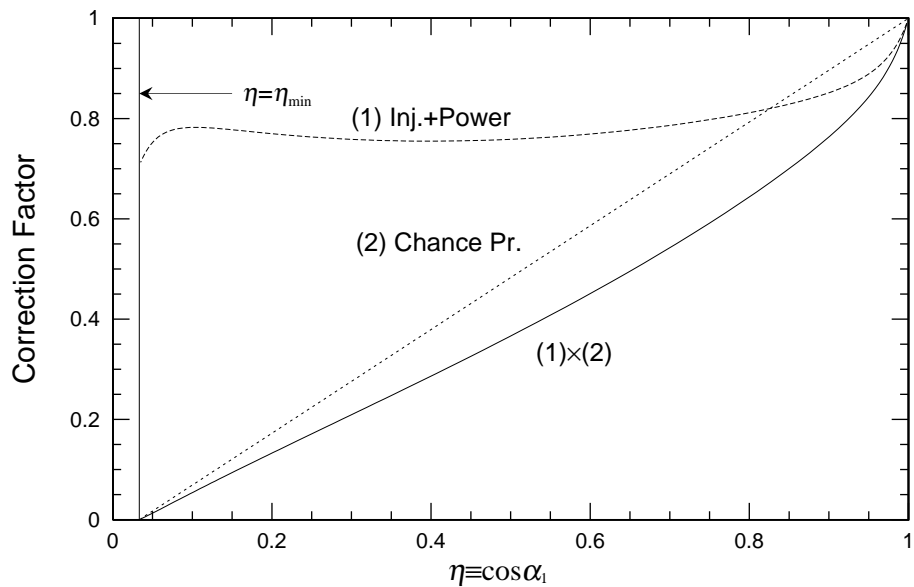


FIG. 3: Correction factors due to the injection efficiency plus the change of index power (dashed), chance probability (dotted) vs. η . The final reduction factor is expressed by the solid curve.

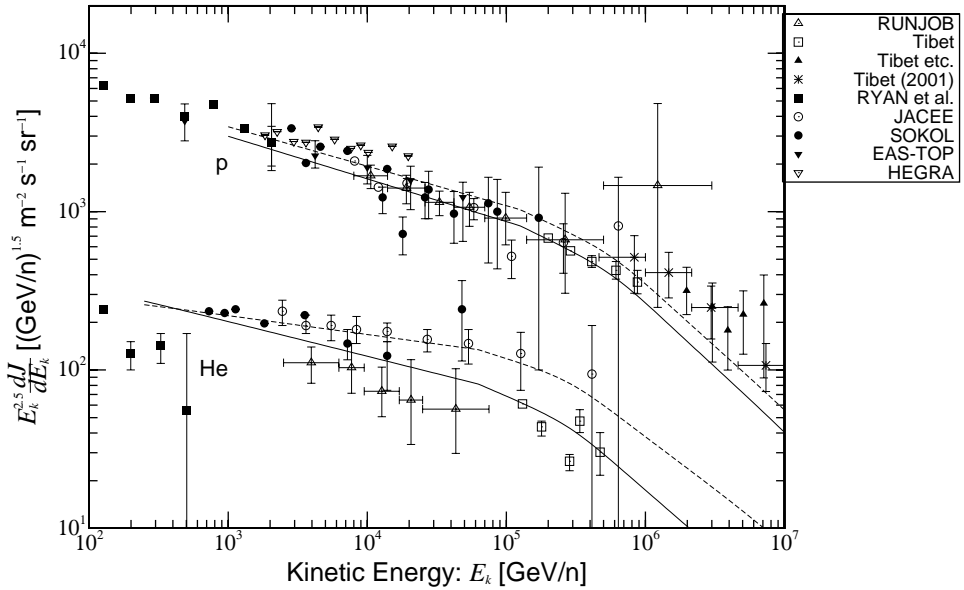


FIG. 4: Comparison of calculated fluxes of p and He with experimental data. The horizontal axis represents kinetic energy per nucleon (GeV/n). The solid and dashed curves represent Ours and HEGRA choices of parameters, respectively as shown in Table I. The original data are RUNJOB [41], Tibet etc. [42], Tibet [43], Tibet (2001) [44], EAS-Top [45], and for others see ref. [41].

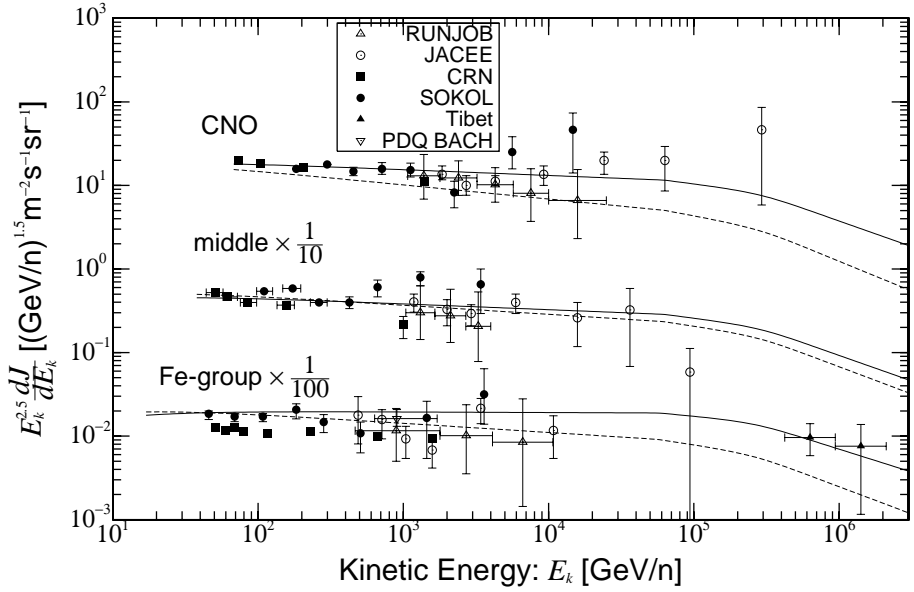


FIG. 5: Comparison of calculated fluxes of CNO-, middle, and Fe-groups with experimental data. The original fluxes of middle and of Fe-group are multiplied by 1/10 and 1/100, respectively. The solid and dashed curves represent the same notation as in Fig. 4. Experimental data are taken from RUNJOB's compilation [41], Tibet [47] and PDQ BACH [48].

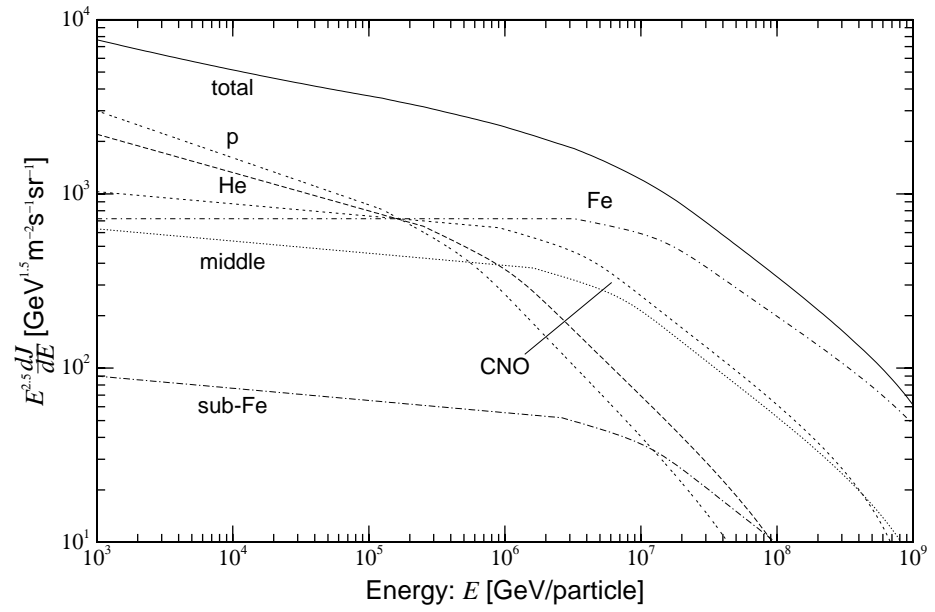


FIG. 6: The predicted fluxes of total, proton, He, and other nuclear groups in the case of “Ours” parameter choices shown in Table I.

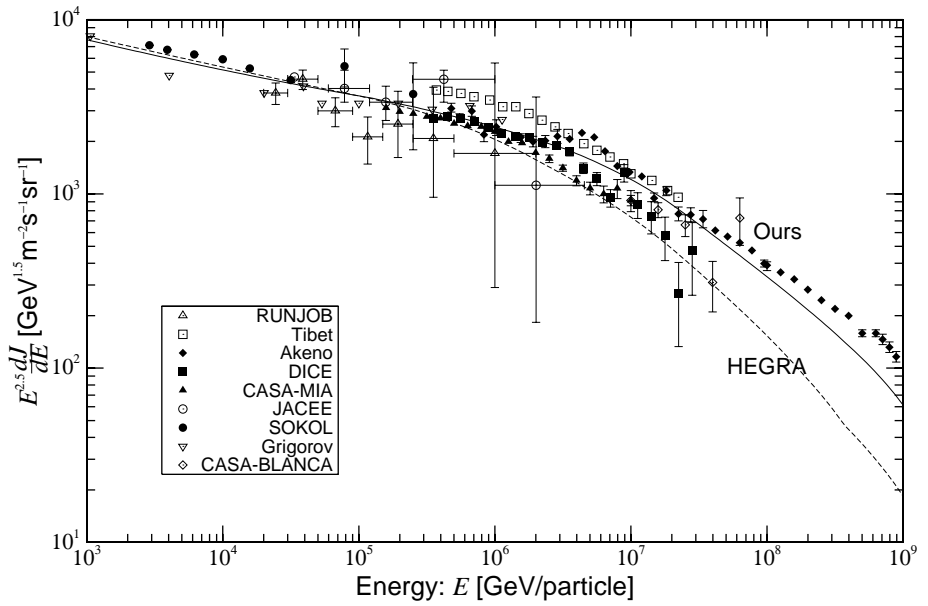


FIG. 7: Comparison of all-particle spectrum versus total energy per particle between experimental data from various groups and the present calculation. The solid and dashed curves represent the same as in Fig. 4. The data are Tibet [42], AKENO [2, 53], DICE [54, 55], CASA-MIA [56] and CASA-BLANCA [3] (here only five data points with higher energies are cited in order to avoid overcrowding since other 16 points of lower energies mostly overlap with CASA-MIA data). Others are cited from RUNJOB's compilation [41].

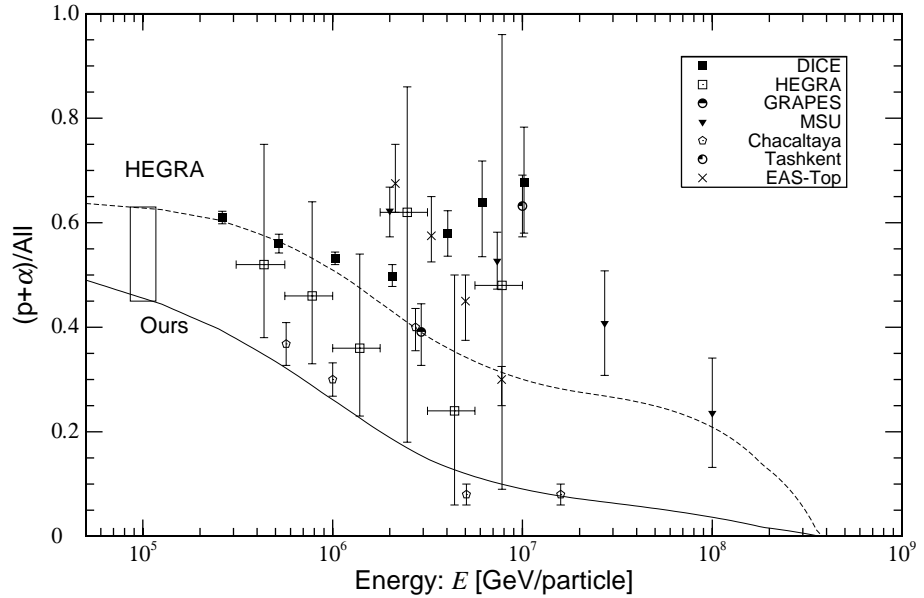


FIG. 8: Energy dependence of $(p + \alpha)/\text{All}$. Two predicted curves which come from two choices of parameters are the same as in Fig. 4. Experimental data are as follows: HEGRA [58], DICE [54], EAS-Top [59], and others are Watson's compilation [60]. The large rectangle area shows direct measurement.

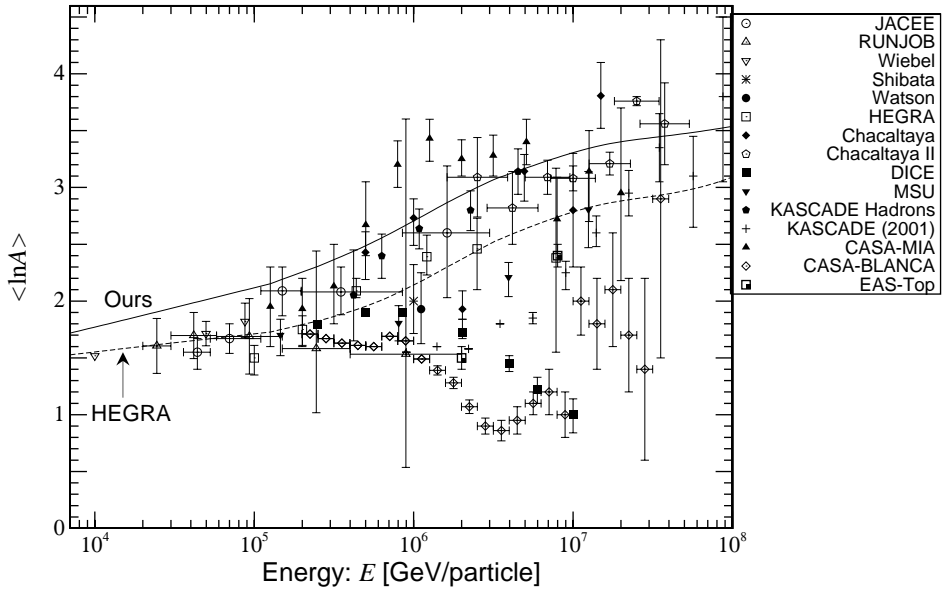


FIG. 9: Energy dependence of chemical composition of primary cosmic rays in term of $\langle \ln A \rangle$. The solid and dashed curves come from Ours and HEGRA choices of parameters, respectively as shown in Table I. Experimental data are as follows: JACEE [46], RUNJOB [41], DICE [54] (X_{\max} +Muon), CASA-MIA [62], CASA-BLANCA (by QGSJET interaction model) [3], EAS-TOP [59], KASCADE hadrons[63], KASCADE (2001) (preliminary data) [57], and Chacaltaya and Chacaltaya II are cited from [64] and [65], respectively. About half of recent data from KASCADE (2001) and Chacaltaya II are plotted to avoid confusion.

TABLE I: Two choices of parameters for calculation at 1 TeV for the absolute value Ψ and index β in the form of Eq. (11). Ψ is in $[\text{GeV}^{1.5} \text{m}^{-2} \text{s}^{-1} \text{sr}^{-1}]$.

Elements	Z	A	Ψ_{HEGRA}	β_{HEGRA}	Ψ_{Ours}	β_{Ours}
p	1.0	1.0	3447	0.25	3000	0.27
He	2.0	4.0	2087	0.12	2200	0.22
CNO	7.26	14.5	885	0.17	1030	0.07
Middle	12.8	25.8	692	0.11	630	0.07
sub-Fe	21.0	45.0	99	0.11	90	0.07
Fe	26.0	55.9	790	0.11	720	0.0
total			8000		7670	

-
- [1] for example, M. Amenomori et al., *Astrophys. J.*, **461**, 408 (1996).
 - [2] for example, M. Nagano et al., *J. Phys.* **G10**, 1295 (1984).
 - [3] L. F. Fortson et al., in *Proceedings of the 26th International Cosmic Ray Conference* Salt Lake City, USA, 1999, Vol. 3, p. 125; J. W. Fowler et al., *Astropar. Phys.*, **15**, 49 (2001).
 - [4] E. Parizot, J. Paul and A. Bykov, in *Proceeding of the 27th International Cosmic Ray Conference* Hamburg, Germany, 2001, Vol. 6, p. 2070.
 - [5] R. Blanford and D. Eichler, *Phys. Rep.* **154**, 1 (1987).
 - [6] T. K. Gaisser, *Cosmic Rays and Particle Physics* Cambridge University Press, (Cambridge, England, 1990).
 - [7] J. R. Jokipii, *Astrophys. J.* **313**, 842 (1987).
 - [8] M. Ostrowski, *Mon. Not. R. Astron. Soc.* **233**, 257 (1988).
 - [9] F. Takahara and T. Terasawa, *Astrophysical Aspect of the Most Energetic Cosmic Rays* edited by M. Nagano and F. Takahara (World Scientific, Singapore, 1991) p.291.
 - [10] K. Kobayakawa, Y. Sato and T. Samura, in *Proceeding of the 26th International Cosmic Ray Conference*, Salt Lake City, USA, 1999, Vol. 4, p. 467.
 - [11] M. G. Baring, D. C. Ellison and F. C. Jones, *Astrophys. J.* **409**, 327 (1993).
 - [12] M. G. Baring, D. C. Ellison and F. C. Jones, *Astrophys. J. Suppl.* **90**, 547 (1994).
 - [13] D. C. Ellison, M. G. Baring and F. C. Jones, *Astrophys. J.* **453**, 873 (1995).
 - [14] M. Ostrowski, *Mon. Not. R. Astron. Soc.* **249**, 551 (1991).
 - [15] M. Ostrowski, *Mon. Not. R. Astron. Soc.* **264**, 248 (1993).
 - [16] T. Naito and F. Takahara, *Prog. Theor. Phys.* **93**, 287 (1995).
 - [17] T. Naito and F. Takahara, *Mon. Not. R. Astron. Soc.* **275**, 1077 (1995).
 - [18] L. O' C. Drury, *Rep. Prog. Phys.* **46**, 973 (1983).
 - [19] J. G. Kirk and A. F. Heavens, *Mon. Not. R. Astron. Soc.* **239**, 995 (1989).
 - [20] P. D. Hudson, *Mon. Not. R. Astron. Soc.* **131**, 23 (1965).
 - [21] P. O. Lagage and C. J. Cesarski, *Astron. Astrophys.* **125**, 249 (1983).
 - [22] E. G. Berezhko, *Astropar. Phys.* **5**, 367 (1996).
 - [23] A. M. Bykov and I. N. Toptygin, in *Proceeding of the 25th International Cosmic Ray Conference* Durban, South Africa, 1997, Vol. 4, p. 365.

- [24] E. G. Klepach et al., in *Proceeding of the 25th International Cosmic Ray Conference* Durban, South Africa, 1997, Vol. 4, p. 501.
- [25] E. G. Berezhko, V. K. Elshin, and L. T. Ksenofotov, *JETP* **109**, 3 (1996).
- [26] S. G. Lucek and A. R. Bell, *Mon. Not. R. Astron. Soc.* **314**, 65 (2000).
- [27] F. Yusef-Zadeh et al., *Astrophys. J.* **466**, L25 (1996).
- [28] M. J. Claussen et al., *Astrophys. J.* **489**, 143 (1997).
- [29] B. Koralesky et al., *Astron. J.* **116**, 1323 (1998).
- [30] C. L. Brogan et al., *Astrophys. J.* **537**, 875 (2000).
- [31] B. Jun and M. L. Norman, *Astrophys. J.* **472**, 245 (1996).
- [32] J. R. Dickel, W. J. M. van Breugel and R. G. Strom, *Astron. J.* **101**, 2151 (1991).
- [33] D. K. Milne, in *IAU Symposium 140, Galactic and Intergalactic Magnetic Fields*, edited by B. Beck, P. P. Kronberg, R. Wielebinski (Kluwer, Dordrecht, 1990), 67.
- [34] M. G. Baring, D. C. Ellison and F. C. Jones, *Astrophys. J.* **453**, 873 (1995).
- [35] D. C. Ellison, F. C. Jones and S. P. Reynolds, *Astrophys. J.* **360**, 702 (1990).
- [36] D. C. Ellison, M. G. Baring and F. C. Jones, *Astrophys. J.* **473**, 1029 (1996).
- [37] D. C. Ellison, *Prog. Theor. Phys. Suppl.* **143**, 125 (2001).
- [38] M. M. Shapiro and M. Silberberg, *Ann. Rev. Nucl. Sci.* **20**, 323 (1970).
- [39] P. Blasi, *Astropar. Phys.* **16**, 429 (2002).
- [40] F. Aharonian et al., *Phys. Rev. D* **59**, 092003 (1999).
- [41] A. V. Apanasenko et al. (RUNJOB collaboration), *Astropar. Phys.* **16**, 13 (2001).
- [42] M. Amenomori et al., (The Tibet AS γ Collaboration), in *Proceeding of the 26th International Cosmic Ray Conference* Salt Lake City, USA, 1999, Vol. 3, p. 211.
- [43] M. Amenomori et al. (The Tibet AS γ Collaboration), *Phys. Rev. D* **62**, 112002 (2000).
- [44] M. Amenomori et al., (The Tibet AS γ Collaboration), in *Proceeding of the 27th International Cosmic Ray Conference* Hamburg, Germany, 2001, Vol. 1, p.18.
- [45] A. Castellina, on behalf of the EAS-TOP COLLABORATION, in *Proceeding of the 27th International Cosmic Ray Conference* Hamburg, Germany, 2001, Vol. 1, p. 3.
- [46] JACEE collaboration, in *Proceeding of the 25th International Cosmic Ray Conference* Durban, South Africa, 1997, Vol. 4 p. 1; JACEE collaboration, *Astrophys. J.* **502**, 278 (1998).
- [47] M. Amenomori et al. (The Tibet AS γ Collaboration), in *Proceeding of the 27th International Cosmic Ray Conference* Hamburg, Germany, 2001, Vol. 1, p. 148.

- [48] J. Clem et al., *Astropar. Phys.* **16**, 387 (2002).
- [49] K. Bernlöhr et al., *Astropar. Phys.* **8**, 253 (1998).
- [50] P. L. Biermann, *Astron. Astrophys.*, **271**, 649 (1993).
- [51] T. Stanev, P. L. Biermann and T. K. Gaisser, *Astron. Astrophys.* **274**, 902 (1993).
- [52] A. D. Erlykin and A. W. Wolfendale, *Advances in Space Research* **27**, 803 (2001).
- [53] M. Nagano et al., *J. Phys.* **G18** 423 (1992).
- [54] S. P. Swordy and D. B. Kieda, in *Proceeding of the 26th International Cosmic Ray Conference* Salt Lake City, USA, 1999, Vol. 3, p. 144; *Astropar. Phys.* **13**, 137 (2000).
- [55] D. B. Kieda and S. P. Swordy, in *Proceeding of the 26th International Cosmic Ray Conference* Salt Lake City, USA, 1999, Vol. 3, p. 191.
- [56] M. A. K. Glasmacher et al., in *Proceeding of the 26th International Cosmic Ray Conference* Salt Lake City, USA, 1999, Vol. 3, p. 199.
- [57] H. Ulrich et al., in *Proceeding of the 27th International Cosmic Ray Conference* Hamburg, Germany, 2001, Vol. 1, p. 97.
- [58] A. Röhrling et al., in *Proceeding of the 26th International Cosmic Ray Conference* Salt Lake City, USA, 1999, Vol. 3, p. 152.
- [59] B. Allesandro for THE EAS-TOP COLLABORATION, in *Proceeding of the 27th International Cosmic Ray Conference* Hamburg, Germany, 2001, Vol. 1, p. 124.
- [60] A. A. Watson, in *Proceeding of the 25th International Cosmic Ray Conference* Durban, South Africa, 1997, Vol. 8, p. 257.
- [61] J. R. Hörandel, in *Proceeding of the 27th International Cosmic Ray Conference* Hamburg, Germany, 2001, Vol. 1, p. 71.
- [62] M. A. K. Glasmacher et al., in *Proceeding of the 26th International Cosmic Ray Conference* Salt Lake City, USA, 1999, Vol. 3, p. 129.
- [63] J. Engler et al., in *Proceeding of the 26th International Cosmic Ray Conference* Salt Lake City, USA, 1999, Vol. 1, p. 349.
- [64] C. Aguirre et al., *Phys. Rev. D* **62**, 032003 (2000).
- [65] S. Ogio et al., in *Proceeding of the 27th International Cosmic Ray Conference* Hamburg, Germany, 2001, Vol. 1, p. 115 and private communication.
- [66] R. J. Protheroe and A. P. Szabo, *Phys. Rev. Lett.* **69**, 2885 (1992).
- [67] C. D. Dermer and M. Humi, *Astrophys. J.* **556**, 479 (2002).